Contents lists available at ScienceDirect

Construction and Building Materials

Freeze-thaw durability of air-entrained high-strength clogging resistant permeable pavements

Alalea Kia [*]

Centre for Infrastructure Materials, Department of Civil and Environmental Engineering, Imperial College London, SW7 2AZ, UK

ARTICLE INFO

ABSTRACT

Permeable concrete pavements are designed to absorb rainfall, however they suffer from a number of challenges, which prevent their widespread adoption. Current permeable pavements are prone to clogging by sediments and have both low strength and durability. A clogging resistant permeable pavement (CRP, also known as Kiacrete) has been developed that has improved permeability, clogging resistance, strength and freeze–thaw durability. This paper reports on the performance of CRPs of the same open porosity made with different pore sizes, pore wall thicknesses and target entraining air content when exposed to 56 freeze–thaw cycles. The tests involved exposing samples to temperature varying from -20 °C to +20 °C and measuring changes in mass, ultrasonic pulse velocity, and compressive and flexural strength. The samples made with the Kiacrete tiles, which is the in-situ delivery method, were also vacuum impregnated and imaged using a stereomicroscope to determine the effect of target entrained air content and freeze–thaw cycles on microcracking. The results show that CRP is highly resistant to freeze–thaw degradation and no further addition of air entraining agent is required. The microcracks that occur do not have any notable impact on the overall durability performance. This study presents the first high strength clogging resistant permeable pavement that is highly durable under frost action, without requiring air entrainment inclusion, enabling permeable concrete pavements to be adopted in cold climates.

1. Introduction

The annual global cost of flooding is projected to increase to £500bn by 2030 from £60bn in 2019 [3,66], with climate change increasing the likelihood of major storm events by 59% [49]. Permeable concrete pavements are one of the most promising flood mitigation strategies as they rapidly drain stormwater through otherwise impermeable infrastructure. Conventional permeable concrete pavements, however, have a number of well-known challenges, they: i) are prone to clogging by sediments; ii) have low compressive (<30 MPa) and flexural (<3.8 MPa) strength; and iii) have low durability due to their high porosity (the volume of large voids that enable water to pass through divided by the total volume) of 15%-35% [15,44,60,59,33,34,35,32,31]. The application of permeable concrete pavements in cold regions has been limited due to their severe deterioration under frost action [56,37,38].

A number of studies have found that whilst the addition of fine aggregates, polypropylene fibres and rubber to pervious concrete mixes improves the freeze–thaw (F-T) performance, they lead to reductions in porosity and permeability, which are the main contributors to the pavement's overall drainage performance [30,69,23,2,19,10,42,46,9]. Silica fume addition of up to 5 wt.% of cement was found to improve the F-T durability, whilst reducing the porosity [28,69]. However, increasing the silica fume replacement rate to >5 wt.% of cement paste led to a dry mixture with increased porosity and reduced F-T durability [28]. Air entrainment improves F-T resistance of permeable concrete pavements by decreasing the hydraulic pressure that develops during the freezing of the pore water [56,28–30,22]. The presence of entrained air voids can, however, lead to further reductions in the compressive strength.

In general concrete infrastructure in cold areas are affected by the F-T damage. One of the most effective ways to improve the concrete F-T durability is by adding air entraining admixture (AEA) to the mix [47,58,43,18,67,64]. AEA introduces air bubbles into the mix, which provides space for the water to freeze as it expands and reduces the internal pressure within the concrete [17]. Sha & Li [57] and Ziaei-Nia et al. [73] have found that adding AEA to concrete improves the pore structure, which reduces the F-T damage. AEA content of 0.01%-0.15% was found to be satisfactory, whilst AEA dosage of >1.5% led to

---

Fig. 1. Large-scale delivery of CRP at Imperial College London's White City Campus.

collapsed pores before the cement paste was hardened [39,64]. AEA was found to reduce the compressive strength of concrete, with typical losses of at least 4–6% being observed with every 1% increase in the entrained air content [51,54,24,8,45,20,55,70,50,62,21,71].

A small number of studies have investigated the relationship between the flexural strength of concrete and the entrained air content of the mix. Toutanji [63] tested concrete mixes of varying silica fume replacement rate (0%-20% wt. cement) with the air content ranging between 2% and 15%, and observed that the AEA reduced both the compressive and flexural strength of silica fume concrete. Conversely, an increase in the entrained air content of up to 7% was found to improve the flexural strength, with the highest flexural strength obtained when the entrained air content is 3%-4% [72]. This increase in the flexural strength is due to the air bubbles in the air entrained concrete occupying water positions at the interfaces, which leads to a more homogenous mix with reduced bleeding and segregation. Furthermore, as cracks slowly grow under the flexural load, the presence of entrained air voids reduces their energy, increasing the resistance to cracking. This is consistent with the findings of Klieger [40], who found the flexural strength to increase with an entrained air content of up to 6%, due to the reductions in water content achieved using AEA. Yang et al. [68] found the flexural strength of concrete to improve with the entrained air content of up to 2.5%, followed by a slow reduction with an entrained air content of up to 7%. These results suggest that the use of AEA in concrete requires careful consideration due to its effects on the mechanical properties and F-T durability.

New types of permeable pavements have been developed to address the previously discussed challenges in conventional permeable pavements. Jones et al. [25] developed concrete beams with drainage holes of 12.5 mm in diameter, 50 mm spacing and porosity of 3.1%. The splitting tensile strength and modulus of rupture of these precast concrete beams were compared with equivalent beams without drainage holes. The strength ratio between the beams with and without the drainage holes was approximately 0.71. A number of issues were noted by Jones et al. [25] in preparing these test specimens, including breakage of the vertical dowels.

A more recent development is high-strength clogging resistant permeable pavement (CRP, also known as Kiacrete), which has improved permeability (>2 cm/s), clogging resistance, strength (>50 MPa) and durability, compared with conventional systems

[34,35,32,37,38]. This enhanced permeability and clogging resistance performance is due to CRP's uniform pore structure of tortuosity of 1, which is prepared by introducing direct pore channels of 3–6 mm diameter in self-compacting mortar. A novel interlocking tile system [36]was developed, to address the challenges of scaling up the innovation, which was recently deployed at scale as cast in-situ slab at the new White City Campus of Imperial College London in the United Kingdom (Fig. 1). This system was shown to be easier to construct on site as it uses self-compacting cementitious material, which unlike the conventional systems does not require placing by specialist contractors to avoid over-compaction or closure of the surface pores [27,1,33,16]. A structural and hydrological design methodology for this system has been reported in Kia et al. (2021). CRP, without any AEA, has been shown to be highly resistant to degradation caused by F-T cycles compared to conventional permeable concrete, reducing the maintenance requirements and improving the service-life [37,38].

The overall aim of this study is to: i) compare CRP samples of the same open pore porosity prepared with different pore diameters (3 mm and 6 mm), pore wall thickness (nominal 0.1 mm and 2 mm) and varying target entrained air contents of 0%, 3% and 6%; ii) assess the effect of AEA on internal microcracks, compressive and flexural strength and durability when exposed to F-T cycles; and iii) determine whether it is necessary to include AEA in CRP when they are used in cold regions. Experimental variables are the pore diameter (3 mm and 6 mm), pore wall thickness (nominal 0.1 mm and 2 mm), target entrained air content (0%, 3% and 6%) and F-T degradation method, used to simulate field temperature and moisture gradients. The results are compared against plain self-compacting mortar of 0% open porosity and varying entrained air content subjected to the same F-T cycles. The measured data in this study will enhance our understanding of the performance of permeable pavements, with and without AEA, when exposed to cyclic freeze–thaw and enable their adoption in cold climates.

2. Experimental program

2.1. Sample preparation

Samples with two different porosities (0% and 7%) were prepared in this study. Three CRP sample types, with constant 7% porosity and target entrained air content of 0%, 3% and 6%, were prepared with self-

Table 1
Mix compositions of 0% porosity solid self-compacting mortar and 7% porosity CRP samples with varying entrained air content.

Sample type	Target entrained air content (%)	No of tubes × diameter of tubes (mm) per 100 mm cube sample	Cement (kg/m³)	Sand (kg/m³)	Water (kg/m³)	SP* (% wt. cement)	AEA** (% wt. cement)	w/c	Open porosity (%)
0%	0	–	711	1323	284	0.4	0.0	0.4	0
	3	–	711	1323	284	1.0	0.2	0.4	0
	6	–	711	1323	284	1.2	0.4	0.4	0
7% 3 mm tubes	0	99 × 3	669	1245	267	0.4	0.0	0.4	7
	3	99 × 3	669	1245	267	1.0	0.2	0.4	7
	6	99 × 3	669	1245	267	1.2	0.4	0.4	7
7% 6 mm tubes	0	25 × 6	669	1245	267	0.4	0.0	0.4	7
	3	25 × 6	669	1245	267	1.0	0.2	0.4	7
	6	25 × 6	669	1245	267	1.2	0.4	0.4	7
7% 6 mm Kiacrete	0	25 × 6	669	1245	267	0.4	0.0	0.4	7
	3	25 × 6	669	1245	267	1.0	0.2	0.4	7
	6	25 × 6	669	1245	267	1.2	0.4	0.4	7

* A polycarboxylic-ether type superplasticiser, MasterGlenium 315C.
** An air-entraining admixture, MasterAir 119.

Fig. 2. Stages of CRP preparation: (a) plastic tubes held in place using a timber base and steel plate at top of the mould; and (b) final ground sample prior to testing.

compacting mortar using: i) the plastic Kiacrete tiles, which was the in-situ delivery method used at the White City field site (6 mm diameter open tubes, 2 mm wall thickness); and ii) plastic tubes of two different diameters (3 mm and 6 mm diameter open tubes, both with nominal 0.1 mm wall thickness). The 0% porosity samples are solid (i.e. impermeable), made from the same self-compacting mortar mix and are compared with the CRP samples as a reference. The self-compacting mortar was prepared using CEM I 52.5 N (711 kg/m³) and fine-grained river sand (<2.5 mm, 1323 kg/m³) at a water/cement (w/c) ratio of 0.40. The specific gravity of the sand was 2.76 and 24-hour absorption was 0.7%. A polycarboxylic-ether type superplasticiser (MasterGlenium 315C) was utilised at 0.4 wt.% of cement to achieve the desired workability. An AEA (MasterAir 119) was used at 0.2 and 0.4 wt. % of cement to achieve the target entrained air contents of 3% and 6%, respectively. The mix compositions of all samples in this study are provided in Table 1. The target entrained air contents were achieved by altering the AEA dosage and measured using: i) the pressure meter method in accordance with ASTM C 231 [4] on fresh air-entrained self-compacting mortar mixes and ii) digital image analysis, the images taken with a stereomicroscope (Olympus SZX10) from a slice of hardened air-entrained samples were analysed using an image processing program (ImageJ) to determine the average number of entrained-air bubbles per surface image area (approximately 500×500 pixels).

The order in which superplasticisers and AEA are added in self-compacting cementitious mixes is critical for achieving adequate air-entrainment. When superplasticisers and AEA are added at the same time to the mix their effectiveness is compromised due to the interaction between these two admixtures. Introducing the superplasticisers before the AEA in the mix is considered to minimise the rate of coalescence/collapse in the air bubbles. The recommended self-compacting mortar mixing procedure [6,53,52], adopted in this study, is to mix the cement

and sand for one minute, followed by adding half of the water to the superplasticiser and then mixing this (with the cement and sand) for one minute. The remaining water is added to the AEA, and then finally mixed (with the cement, sand, water and superplasticiser) for two minutes.

Following mixing, the CRP samples were cast in 100 × 100 × 100 mm cubes (or 100 × 100 × 500 mm prisms for flexural strength testing), with the plastic tubes held in place using a 15 mm thick timber base and a steel plate at the top of the mould (Fig. 2a). The plastic Kiacrete tiles were cut to size and placed on top of a 15 mm thick timber base, such that all samples had the same cast 85 mm depth. All samples were trimmed/ground, to remove excess protruding plastic tubes, reducing their height to ~80 mm and leaving a flat surface for testing (Fig. 2b). In total 123 CRP samples were prepared, comprising of 87 100 × 100 × 80 mm cubes and 36 100 × 80 × 500 mm prisms. The 100 × 100 × 80 mm cubes consisted of three replicates for: i) F-T samples (36 specimens, see Table 1) and ii) control samples (not exposed to F-T, 36 specimens, see Table 1), along with five replicates of the Kiacrete target entrained air content mixes for image analysis (15 specimens, see Table 1 and Section 2.3). The 100 × 80 × 500 mm prisms consisted of three replicates for each mix combination in Table 1.

All samples were cast and cured in accordance with BS ISO 1920-3:2019 (British Standards [12]. For the first 24 h, all samples were covered with a wet hessian and polyethylene sheet. The control cube and the prism specimens were then demoulded and placed in a fog room at 20 °C, 95% ± 5% RH until they were tested for compressive and flexural strength respectively. The F-T samples were de-moulded, weighed, wrapped in a plastic film (to ensure that they are moisture-tight) and stored in a room at 20 °C for 6 days. On the following day, the F-T samples were removed from the plastic film, weighed and placed in a 20 °C water bath for 21 days. At 28 days after casting, the F-T specimens
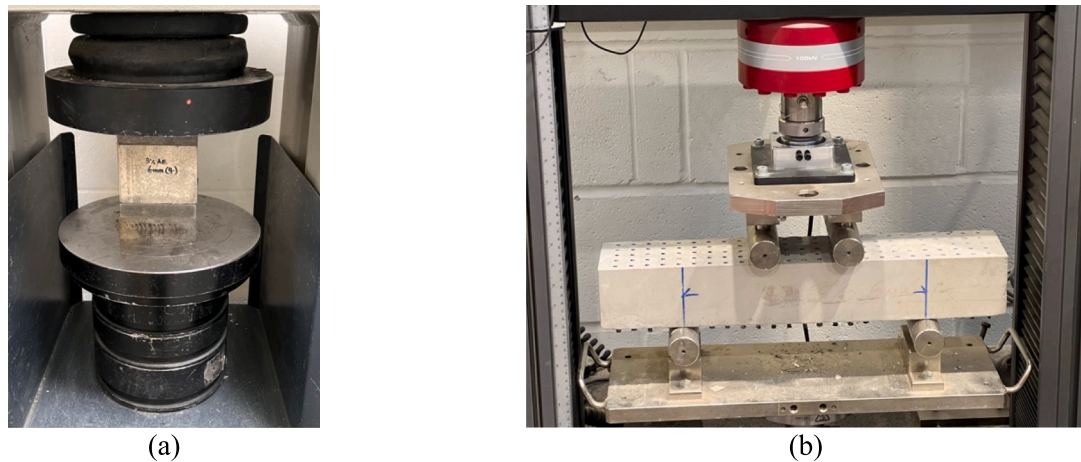
(a)   (b)

Fig. 3. CRP samples are tested for (a) compressive strength and (b) flexural strength.

were removed from the water bath, surface dried with a towel and weighed. This value was used as the mass of the sample at cycle 0.

2.2. Porosity

The porosity of the CRP samples was calculated from the size and number of straight pores (plastic tubes) in the specimen using Equation (1).

$$\phi = \frac{V_p n}{V_c} \times 100\% \tag{1}$$

where ϕ is porosity (expressed as a percentage), V_p is the volume of each pore, n is number of pores and V_c is the sample volume [35]. The calculated porosity values were confirmed experimentally by filling the individual pores with water and dividing its volume by the volume of the sample. The experimentally measured porosity was recorded on 6 replicates per mix and averaged.

2.3. Cyclic freeze–thaw (F-T)

The F-T testing was conducted in accordance with CEN/TR 15177:2006 [11]. The samples were subjected to freezing and thawing under drained conditions, with one F-T cycle undertaken per day. This method is considered to be more representative of the field conditions for permeable concrete pavements [7,48,56,1]. Each cycle consisted of freezing at -20 °C for 8 h followed by thawing in a water tank at +20 °C for 4 h. The samples were manually moved between the freezer and the water tank, due to the absence of an automated environmental chamber. After thawing, the saturated samples were surface dried with a towel, weighed and then their ultrasonic pulse velocity (UPV) was measured. The change in mass and UPV were used to characterise the deterioration rate under freezing and thawing cycles. All of the samples were exposed to the recommended total of 56 F-T cycles [11]. F-T cycles 1, 12, 36 and 56 were previously observed to have significant deterioration in conventional permeable concrete samples [38]. Therefore, in this study Kiacrete samples with target entrained air contents 0%, 3%, 6% were prepared and imaged for microcracking at these identified cycles, along with cycle 0 for comparison (15 samples in total).

2.4. Ultrasonic pulse velocity

The ultrasonic pulse velocity was measured using a 54 kHz P-wave transducer (Proceq Pundit 200) in accordance with ASTM C597-16 [5] on all F-T samples. UPV measurements were taken at five locations on opposite faces of the cube, except the top and bottom faces (i.e. 10 measurements per cube). Petroleum jelly was used as a coupling agent

between the transducer and sample surface, to achieve a stable UPV reading. Measurements were carried out after every F-T cycle and the mean value per mix combination was calculated to detect microstructural changes and potential degradation. Deterioration in the form of micro and macro cracking increases the actual path length for an ultrasonic pulse. In a deteriorated sample, the pulse propagation time from transmitter to receiver is increased, compared with an assumed straight path, causing a reduction in the measured velocity.

2.5. Epoxy impregnation for image analysis

The microcracks were vacuum-impregnated with a fluorescent dyed epoxy resin, in accordance with the procedure detailed in [65]with modifications described herein, and imaged. Epoxy impregnation enables all cracks to be infilled, allowing them to be differentiated from the rest of the sample. After attaining the required number of F-T cycles (0, 1, 12, 36, 56), the $100 \times 100 \times 100$ mm Kiacrete F-T samples were cut into $100 \times 100 \times 30$ mm sections and oven dried at 30 °C, until they reached an equilibrium mass. The bottom 15 mm of the dried samples were then cast in a clear epoxy resin. Once the resin had reached sufficient hardness, the samples were individually placed under a vacuum for 2 h to ensure that all microcracks were completely de-aired. Whilst under vacuum, a low viscosity fluorescent resin (diluted with 5 wt.% of toluene) was poured onto each sample, covering the entire surface. The vacuum was slowly released and the sample was moved to a separate pressure chamber, at 2.5 bars above atmospheric pressure using an oxygen gas bottle, for an additional 2 h. The sample was taken out of the pressure chamber to remove the unhardened excess resin from the sample surface, before being placed back in the chamber and pressurised under the same conditions overnight. The following day, the sample was ground with coarse silicon carbide paper (grit size 80), to remove the hardened resin from the surface. The surface was cleaned, using acetone to remove any leftover grinding material, and then imaged using a stereomicroscope (Olympus SZX10) under fluorescent light. ImageJ was used to visualise the crack patterns with varying F-T cycles and target entrained air content, along with measuring the overall crack length for each cycle.

2.6. Compressive strength

Compressive strength was measured using a compression testing machine (Controls Automax 5) in accordance with BS EN 12390–3:2019 [13]. Samples were placed between $100 \times 100 \times 25$ mm metal plates and loaded at a rate of 0.3 MPa/s to ultimate failure, as shown in Fig. 3a. All control and F-T samples ($100 \times 100 \times 80$ mm) were tested at the same time upon the completion of the F-T testing.
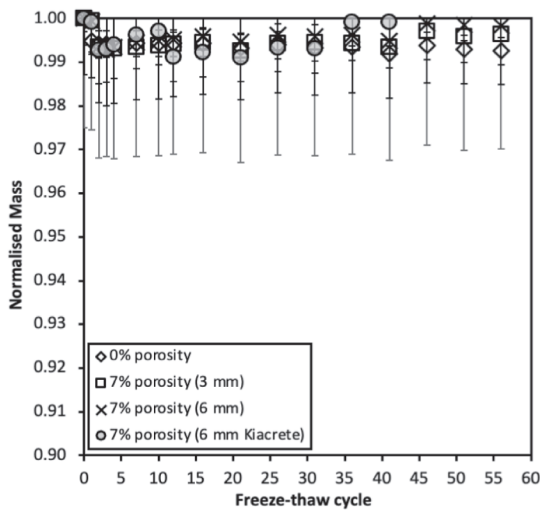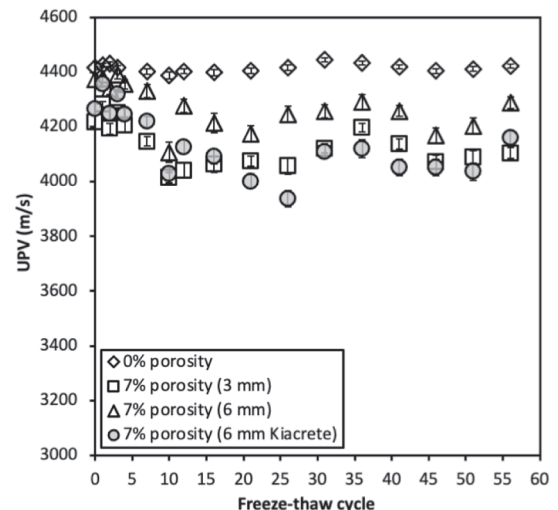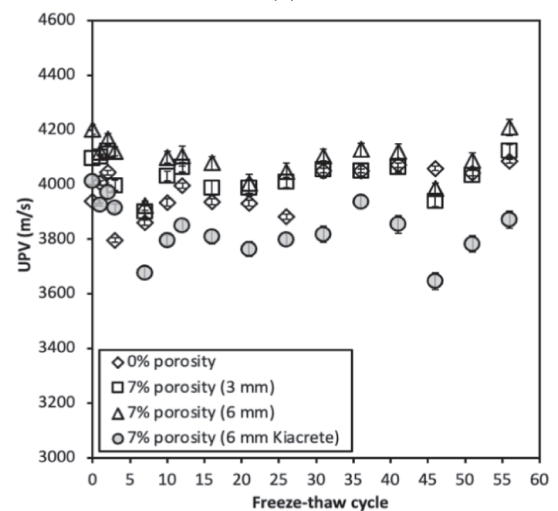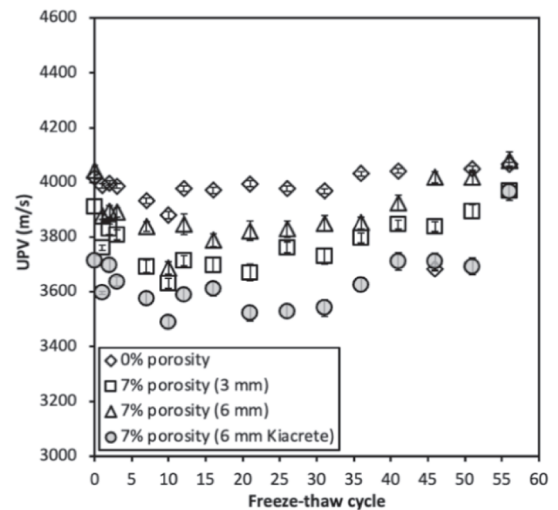
(a)
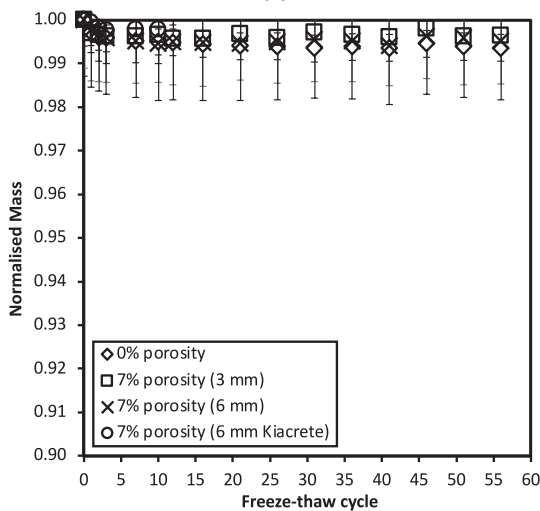
(b)
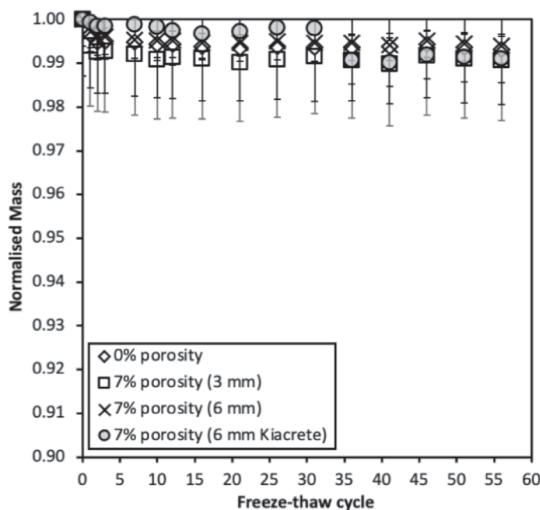
(c)

Fig. 4. Normalised mass against F-T cycles for solid self-compacting mortar and CRP samples of (a) 0% air content, (b) 3% air content and (c) 6% air content.

(a)

(b)

(c)

Fig. 5. UPV against F-T cycles for solid self-compacting mortar and CRP samples of (a) 0% air content, (b) 3% air content and (c) 6% air content.
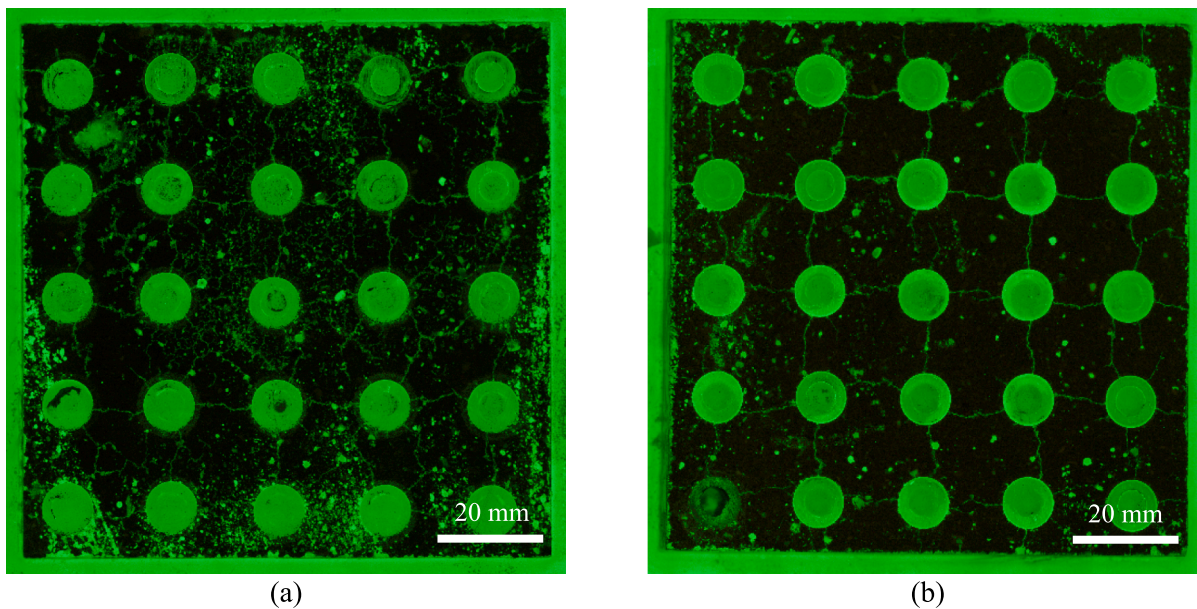
Fig. 6. Stereomicroscope image of an epoxy impregnated Kiacrete sample of 0% air content at (a) cycle 0 and (b) after exposure to 56 F-T cycles.

2.7. Flexural strength

Flexural strength (also known as bending stress or modulus of rupture) was measured using a four-point bending test setup in accordance with BS EN 12390–5:2019 (British Standards [14]. 100 × 80 × 500 mm prisms were tested at 28 days in an Instron 5982 machine (Fig. 3b). The flexural strength of a beam can be calculated using Equation (2).

$$f_{cf} = \frac{My}{I} \tag{2}$$

where f_{cf} is the flexural strength, M is the bending moment, y is the distance from the neutral axis to the extreme fibres and I is the second moment of area.

The four-point bending loading configuration in BS EN 12390–5:2019 (British Standards [14] has the distance 'between the loading rollers' and 'between the supporting roller and loading roller' as

the beam width. Substituting this distance, along with the total applied load, the second moment of area and the distance from the neutral axis to the extreme fibres, into Equation (2), results in the flexural strength expression from BS EN 12390–5:2019 (British Standards [14]:

$$f_{cf} = \frac{FL}{bd^2} \tag{3}$$

where F is the maximum load, L is the distance between supporting rollers (=3b), b is the sample width and d is the sample depth.

3. Results and discussion

3.1. Mass loss

Figs. 4a-c show the averaged normalised sample mass (mass in each cycle divided by the initial mass) varying with the F-T cycle for samples with target entrained air contents of 0%, 3% and 6% respectively.
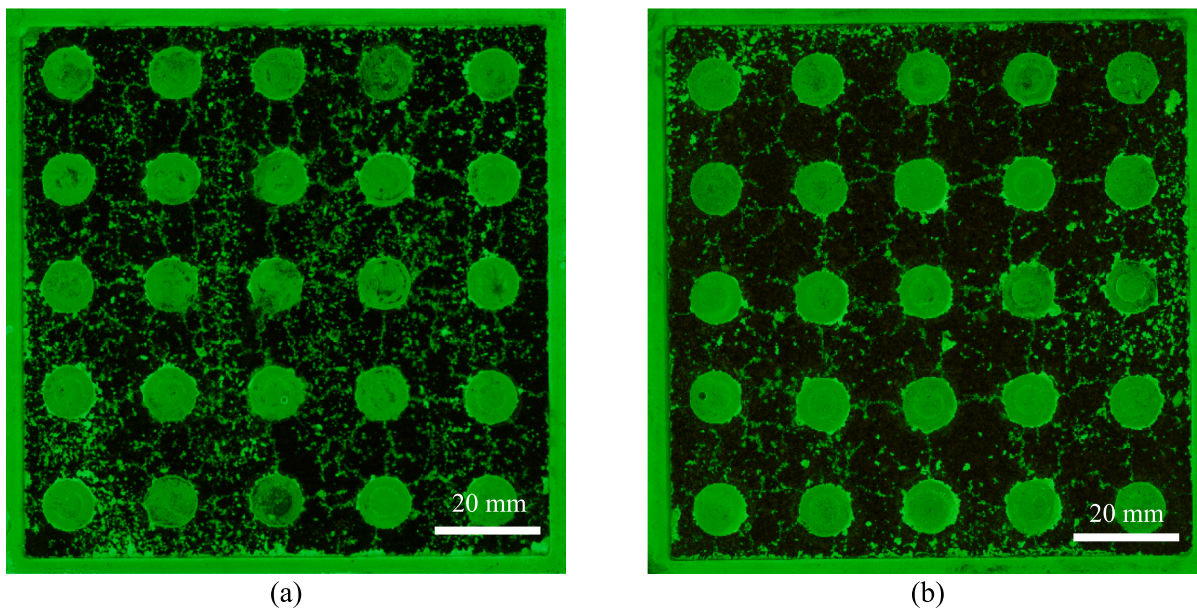

Fig. 7. Stereomicroscope image of an epoxy impregnated Kiacrete sample of 3% air content at (a) cycle 0 and (b) after exposure to 56 F-T cycles.
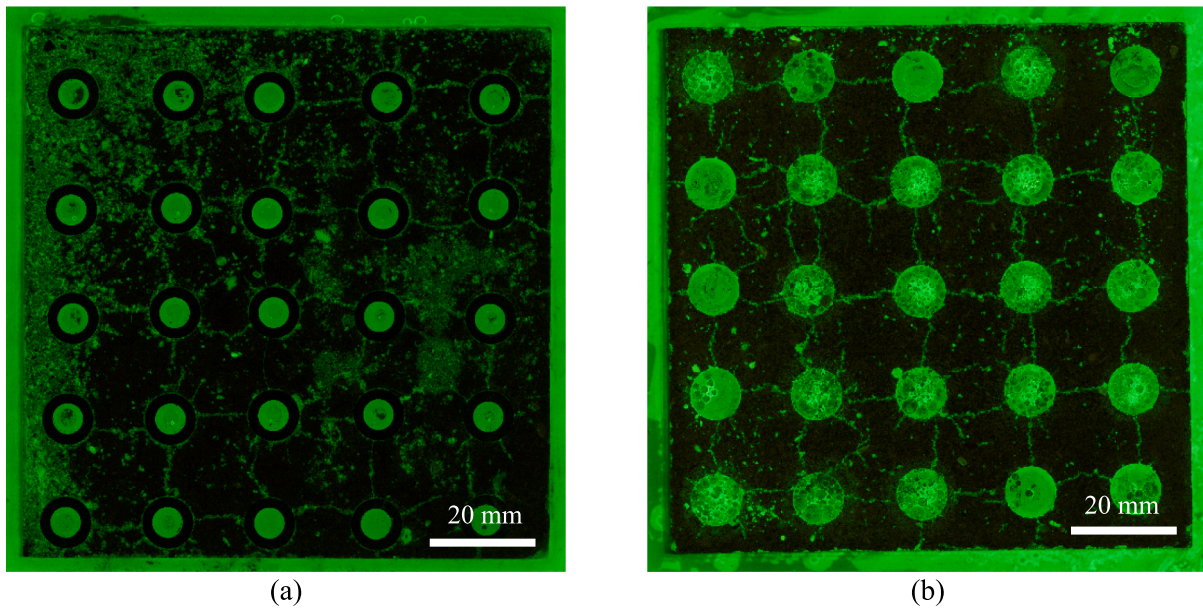
(a)   (b)

Fig. 8. Stereomicroscope image of an epoxy impregnated Kiacrete sample of 6% air content at (a) cycle 0 and (b) after exposure to 56 F-T cycles.

Table 2
Overall crack length of Kiacrete samples with varying entrained air content at different F-T cycles.

Target entrained air content (%)	0	3	6
F-T cycle number	**Crack length (mm)**		
0	200.8	198.0	196.1
1	192.5	203.8	200.6
12	208.5	205.5	195.5
36	196.5	206.0	199.8
56	197.2	202.5	210.5

Minimal mass loss (<1%) was observed across all samples, which is attributed to the superplasticiser in the self-compacting mortar mix. The superplasticiser reduces the surface tension of the paste liquid phase and increases the air content of the mortar [61,41]. This effect enables the samples with 0% target entrained air content to have the same F-T resistance, as those that used AEA. The presence of the pores in CRP does not affect the F-T performance as observed in the mass loss of the 7% CRP and 0% solid samples. Furthermore, the different pore diameters (3 mm and 6 mm) and pore wall thicknesses (nominal 0.1 mm and 2 mm) did not influence the F-T performance between the 7% porosity CRP samples.

3.2. Ultrasonic pulse velocity (UPV)

Figs. 5a-c show the change in average UPV with the F-T cycle, with no significant UPV reductions observed across all samples. Similar to the mass loss results (see Section 3.1), the F-T performance, as indicated by UPV, was not affected by the porosity of the samples. The average UPV values of the samples with 0% target air content was 6% higher than the samples with 3% target air content and 10% higher than the ones with 6% target air content. This is due to the presence of air bubbles from the AEA resulting in a longer true path length for the ultrasonic pulse, thus reducing the UPV values with an increase in the air content.

3.3. Micro cracking observation using imaging

No degradation (significant difference between the microcracks) was observed, through visual inspection and overall crack length measurements, over cycles 0, 1, 12, 36 and 56. Therefore, only cycles 0 and 56
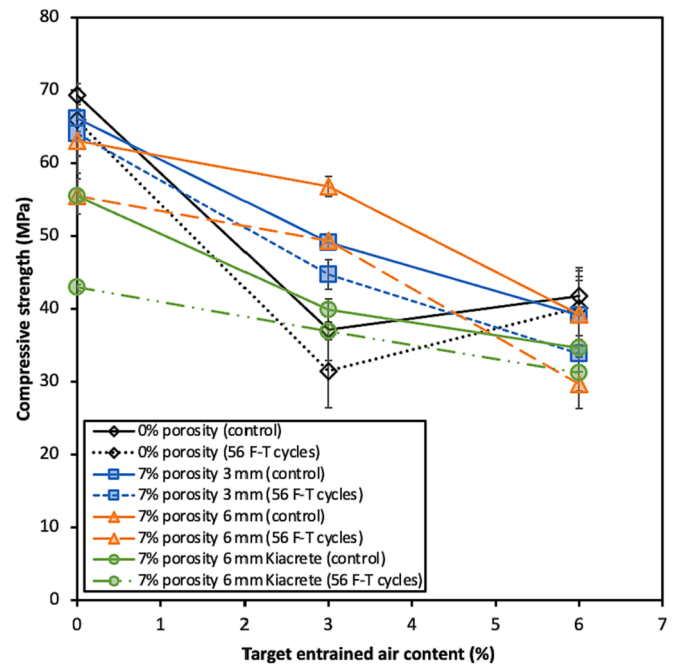

Fig. 9. Compressive strength against air content for control and 56 F-T cycles exposed solid self-compacting mortar and CRP samples.

are presented in Figs. 6-8 for Kiacrete samples of 0%, 3% and 6% target entrained air content. In 3% and 6% target air content samples the resin has penetrated deep into the mortar pores, due to their more porous nature, making it more challenging to observe the microcrack patterns. From Figs. 6-8 and Table 2, it is apparent that the microcracks did not change significantly across the 56 F-T cycles. Furthermore, for target entrained air contents of 0% and 3%, the largest crack length was not observed for the samples exposed to the maximum number of F-T cycles, indicating that the Kiacrete samples have a good overall F-T durability performance. The presence of the cracks at cycle 0 suggests that they were caused during the sample preparation process (e.g. cutting or grinding the top surface) rather than being caused by the F-T cycles. The microcracks in 3% and 6% target entrained air content samples were
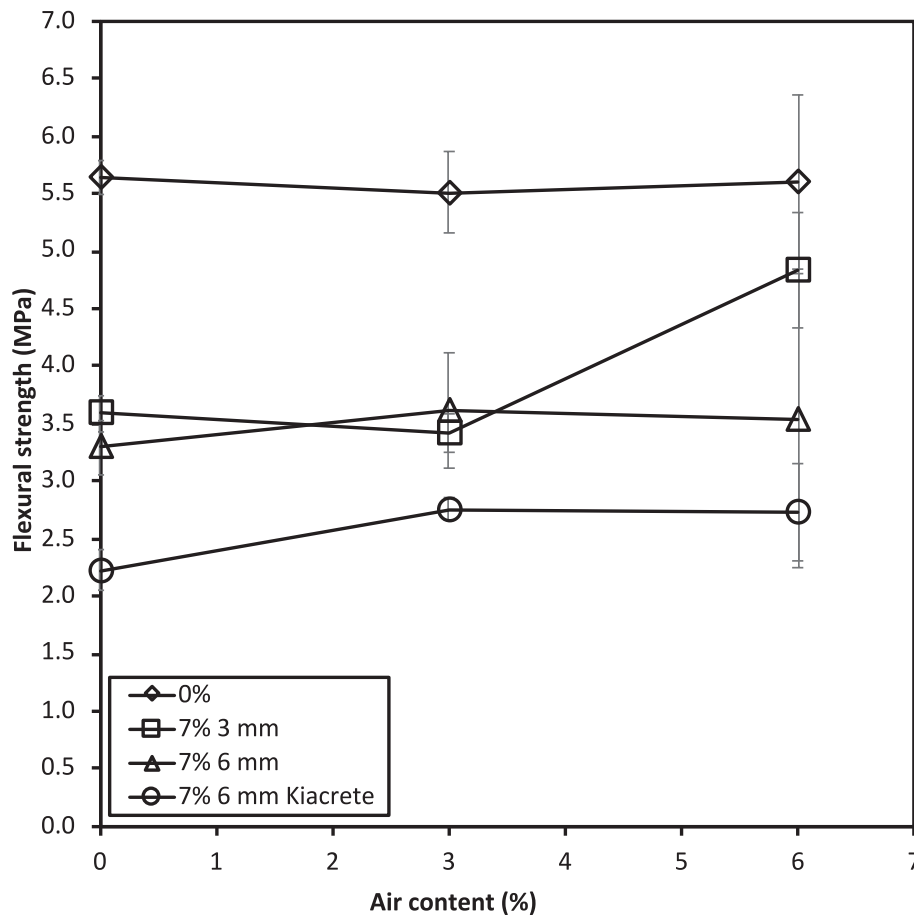
Fig. 10. Flexural strength against air content for solid self-compacting mortar and CRP samples.

formed radially around the direct pore channels, similar to the samples with 0% target air content, creating a microcrack network with the adjacent pores. This observation suggests that the superplasticiser used in the self-compacting mortar mix is sufficient for providing F-T resistance, therefore no AEA addition is required in CRP.

3.4. Compressive strength

The strength and porosity of a permeable concrete pavement is closely related to its F-T durability. Fig. 9 presents the compressive strength against the target entrained air content for all control and F-T exposed samples. The reported compressive strength for the 7% porosity sample types utilises the combined area of mortar and plastic in its calculation, to account for the varying total pore area. The average compressive strength for the control samples ranged from 35 MPa to 69 MPa. The average compressive strength of the samples exposed to 56 F-T cycles was comparable to that of the control samples, ranging from 30 MPa to 66 MPa, indicating that the F-T cycles had no significant impact (~10% reduction in average compressive strength) on the mechanical properties of CRP. The average compressive strength reduction after exposure to 56 F-T cycles for samples of 0%, 3% and 6% target entrained air content was 10%, 11% and 13% respectively. The 0% and 7% CRP samples made with 3 mm tubes had an average compressive strength reduction of 8%, whilst this was 16% and 13% respectively for 7% porosity CRP samples made with 6 mm tubes and 6 mm Kiacrete. As expected, the compressive strength reduced with an increased target entrained air content for both the control and F-T exposed CRP samples. The 3 mm and 6 mm samples exhibited slightly higher compressive strength than the Kiacrete samples, which is attributed to the greater proportion of plastic to mortar within the latter specimens.
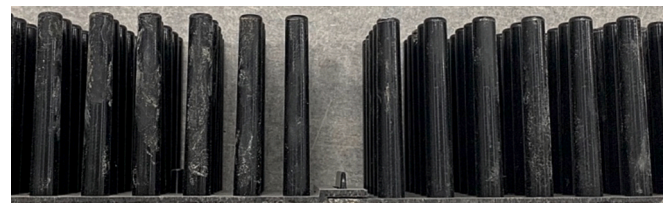

Fig. 11. A close-up view of the central joint in the Kiacrete plastic tile.

3.5. Flexural strength

The flexural strength as a function of the target entrained air content for solid self-compacting mortar and CRP samples, is shown in Fig. 10. The reported flexural strength for the 7% porosity sample types takes into account the reduction in beam width due to the pores in its calculation. The flexural strength ranged from 3.5 MPa to 6.6 MPa for all samples. The solid self-compacting mortar samples exhibited the highest flexural strength values, apart from at 6% target entrained air content. The CRP samples made with 3 mm tubes had slightly higher flexural strength than those with 6 mm diameter tubes. This is because decreasing the tube diameter led to an improved interlocking action, which meant that the fracture had to propagate through a thicker mortar matrix. Furthermore, the Kiacrete samples had the lowest flexural strength values, which is believed to be due to the presence of a 12 mm deep joint (that joins the separate plastic Kiacrete tiles together) at the centre of these samples (Fig. 11), protruding into the mortar and acting like a flaw. The ultimate failure for all Kiacrete samples consistently occurred at this central joint (Fig. 12a), whereas the location of the
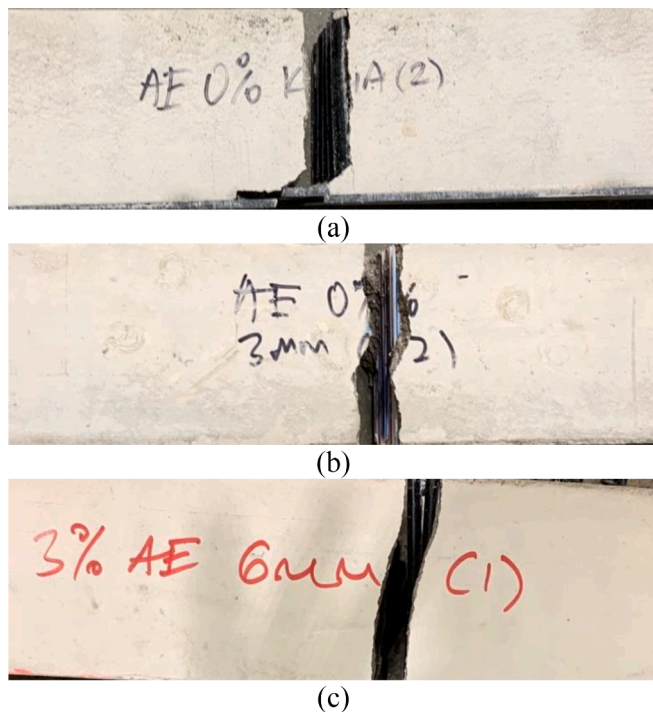
(a)

(b)

(c)

Fig. 12. A close-up view of the failure modes for CRP samples made with: (a) the Kiacrete plastic tile; (b) 3 mm diameter tubes and (c) 6 mm diameter tubes.

failure plane varied for the CRP samples with 3 mm and 6 mm diameter tubes, however it was always along a vertical tube (Fig. 12b-c). The flexural strength, unlike the compressive strength, did not change significantly with an increase in the target entrained air content, but it was slightly higher for samples with target air contents of 3% or 6% in comparison to those with 0%. This slight increase is believed to be due to the presence of the air bubbles: i) leading to a more homogenous cementitious mixture; and ii) increasing the resistance to cracking by absorbing the crack growth energy, which is consistent with the findings of Klieger [40] and Zheng et al. [72].

4. Conclusions

The F-T durability of solid self-compacting mortar and CRP samples made with varying pore diameters and wall thickness, with different target entrained air content, was tested and compared. All F-T samples were exposed to temperature varying from -20 °C to +20 °C and changes in mass, UPV, and compressive strength were measured. The effect of target entrained air content and F-T cycles on the microcracks was determined by vacuum impregnating and imaging the samples using a stereomicroscope. The flexural strength of all sample types with varying target entrained air content was also measured. The test variables were the pore diameter (3 mm and 6 mm), pore wall thickness (nominal 0.1 mm and 2 mm), target entrained air content (0%, 3% and 6%) and the F-T degradation method used to simulate temperature and moisture gradients experienced in the field.

The CRP samples of different target entrained air content (0%, 3% and 6%) were observed to be very durable, with minimal mass loss and UPV reductions occurring over the 56 F-T cycles. This is due to CRP's engineered pore structure resulting in high permeability, whilst still achieving high strength and F-T durability. The microcracks in CRP samples, prepared with the Kiacrete plastic tiles, were observed to form a radial network with the adjacent pores from cycle 0. No change in the microcrack network was seen over the 56 F-T cycles, which coupled with the crack length measurements, indicates that they were generated during the sample preparation process rather than being caused by F-T

degradation. The microcracks did not have any notable impact on the overall F-T durability performance. The excellent 0% target entrained air content performance (mass loss, UPV, microcracks) compared with the 3% and 6% target entrained air content, is attributed to the polycarboxylic-ether type superplasticiser used in the self-compacting mortar, reducing the paste surface tension and increasing the mortar air content. The results suggest that the superplasticiser used in the self-compacting mortar mix is sufficient for providing F-T resistance and no further addition of AEA is required.

The compressive strength of control samples was comparable to those exposed to 56F-T cycles, indicating that the F-T cycles had no significant impact on the mechanical properties. As expected, the compressive strength reduced with an increase in the target entrained air content for all samples. The flexural strength of samples with 3% and 6% target entrained air content was slightly higher than those with 0% target entrained air content. This is due to the presence of the air bubbles creating a more homogenous mixture, whilst absorbing the crack growth energy and increasing the resistance to cracking. Without AEA sufficient flexural strength is available and the compressive strength capacity is enhanced, therefore it is recommended to exclude the use of AEA in CRP.

CRP is the first permeable pavement to have high strength, permeability and clogging resistance, whilst being less susceptible to degradation caused by extreme temperature and moisture gradients during F-T cycles, even without the inclusion of AEAs. CRP has the potential to be used in extreme environments without requiring regular maintenance, enabling the widespread adoption of permeable pavements in cold climates.

Declaration of Competing Interest

The authors declare that they have no known competing financial interests or personal relationships that could have appeared to influence the work reported in this paper.

Data availability

All experimental and analytical test data used in this study appear in the submitted article.

Acknowledgements

References

[1] ACI, *Report on Pervious Concrete*. ACI 522R–10, American Concrete Institute (ACI) Committee 522 (2010) 1–38.

[2] A.M. Amde, S. Rogge, Development of high quality pervious concrete specifications for Maryland conditions, State Highway Administration Maryland Department of Transportation, Baltimore, MD, USA, 2013. MD-13-SP009B4F.

[3] Aon 2020. *Economic losses from natural disasters*.

[4] ASTM International ASTM C231-17a Standard Test Method for Air Content of Freshly Mixed Concrete by the Pressure Method. West Conshohocken, PA, ASTM International.

[5] ASTM International, ASTM C597–16 Standard Test Method for Pulse Velocity Through Concrete, West Conshohocken, PA, ASTM International, 2016.

[6] A. Attachaiyawuth, S. Rath, K. Tanaka, M. Ouchi, Improvement of Self-Compactability of Air-Enhanced Self-Compacting Concrete with Fine Entrained Air, Journal of Advanced Concrete Technology 14 (3) (2016) 55–69.

[7] E. Attiogbe, Predicting Freeze-Thaw Durability of Concrete: A New Approach, ACI Materials Journal 93 (5) (1996) 457–464.

[8] M. Barfield, N. Ghafoori, Air-entrained self-consolidating concrete: A study of admixture sources, Construction and Building Materials 26 (1) (2012) 490–496.

[9] H. Bilal, T. Chen, M. Ren, X. Gao, A. Su, Influence of silica fume, metakaolin & SBR latex on strength and durability performance of pervious concrete, Construction and Building Materials 275 (2021), 122124.

[10] A. Bonicelli, F. Giustozzi, M. Crispino, Experimental study on the effects of fine sand addition on differentially compacted pervious concrete, Construction and Building Materials 91 (2015) 102–110.

[11] British Standards Institution, CEN/TR 15177: 2006 Testing the freeze-thaw resistance of concrete - Internal structural damage, British Standards Institution, 2006.

[12] British Standards Institution (2019a). BS ISO 1920-3:2019 Testing of concrete - Part 3: Making and curing test specimens, British Standards Institution.

[13] British Standards Institution, BS EN 12390–3: 2019 Testing hardened concrete, Part 3: Compressive Strength of Test Specimens, British Standards Institution, 2019.

[14] British Standards Institution (2019c). BS EN 12390-5:2019 Testing hardened concrete, Part 5: Flexural Strength of Test Specimens.

[15] J.P. Coughlin, C.D. Campbell, D.C. Mays, Infiltration and clogging by sand and clay in a pervious concrete pavement system, Journal of Hydraulic Engineering 17 (1) (2012) 68–73.

[16] B. Debnath, P.P. Sarkar, Pervious concrete as an alternative pavement strategy: a state-of-the-art review, International Journal of Pavement Engineering 21 (12) (2020) 1516–1531.

[17] K. Ebrahimi, M.J. Daiezadeh, M. Zakertabrizi, F. Zahmatkesh, A. Habibnejad Korayem, A review of the impact of micro- and nanoparticles on freeze-thaw durability of hardened concrete: Mechanism perspective, Construction and Building Materials 186 (2018) 1105–1113.

[18] M.A. Farooq, Y. Sato, K. Niitani, Experimental investigation of monotonic behavior and stress-strain models of AE and non-AE high strength concrete with BFS fine aggregates under freezing and thawing, Construction and Building Materials 249 (2020), 118679.

[19] M. Gesoğlu, E. Güneyisi, G. Khoshnaw, S. İpek, Abrasion and freezing–thawing resistance of pervious concretes containing waste rubbers, Construction and Building Materials 73 (2014) 19–24.

[20] S. Guo, Q. Dai, X. Sun, Y. Sun, Z. Liu, Ultrasonic techniques for air void size distribution and property evaluation in both early-age and hardened concrete samples, Applied Sciences 7 (3) (2017) 290.

[21] M. Hang, L. Cui, J. Wu, Z. Sun, Freezing-thawing damage characteristics and calculation models of aerated concrete, Journal of Building Engineering 28 (2020), 101072.

[22] V. Henderson, S. Tighe, Evaluation of pervious concrete pavement performance in cold weather climates, International Journal of Pavement Engineering 13 (3) (2012) 197–208.

[23] J. Huang, C. Valeo, J. He, A. Chu, Winter performance of inter-locking pavers - stormwater quantity and quality, Water 4 (4) (2012) 995–1008.

[24] W.-R. Huang, D.-B. Yang, J.-T. Zhou, Effects of admixtures and air entraining agent on performance of concrete, Hunningtu(Concrete) 9 (2010) 80–82.

[25] D. Jones, J. Harvey, R. Wang, B. Campbell. *Laboratory Testing and Modeling for Structural Performance of Fully Permeable Pavements: Final Report*, Sacramento, California, California Department of Transportation, 2010, pp. 1–214.

[27] J.T. Kevern, V.R. Schaefer, K. Wang, Evaluation of pervious concrete workability using gyratory compaction, Journal of Materials in Civil Engineering 21 (2009) 764–770.

[28] J.T. Kevern, V.R. Schaefer, K. Wang, M.T. Suleiman, Pervious Concrete Mixture Proportions for Improved Freeze-Thaw Durability, Journal of ASTM International 5 (2) (2008) 1–12.

[29] J.T. Kevern, K. Wang, V.R. Schaefer, Pervious Concrete in Severe Exposures, Concrete International. 30 (2008) 43–49.

[30] J.T. Kevern, K. Wang, V.R. Schaefer, Effect of coarse aggregate on the freeze-thaw durability of pervious concrete, Journal of Materials in Civil Engineering 22 (5) (2010) 469–475.

[31] A. Kia, Permeable concrete pavements for a climate change resilient built environment, in: F. Pacheco-Torgal, C.G. Granqvist (Eds.), Adapting the Built Environment for Climate Change, Publishing, Cambridge, USA, Woodhead, 2023, pp. 297–326.

[32] A. Kia, J.M. Delens, H.S. Wong, C.R. Cheeseman, Structural and hydrological design of permeable concrete pavements, Case Studies in Construction Materials 15 (2021) e00564.

[33] A. Kia, H.S. Wong, C.R. Cheeseman, Clogging in permeable concrete: A review, Journal of Environmental Management 193 (2017) 221–233.

[34] A. Kia, H.S. Wong, C.R. Cheeseman, Defining Clogging Potential for Permeable Concrete, Journal of Environmental Management 220 (2018) 44–53.

[35] A. Kia, H.S. Wong, C.R. Cheeseman, High-Strength Clogging Resistant Permeable Pavement, International Journal of Pavement Engineering 2019 (2019) 1–20.

[36] Kia, A., Wong, H. S. and Cheeseman, C. R. (2020). High strength porous cement-based materials.

[37] Kia, A., Wong, H. S. and Cheeseman, C. R. (2021b). Freeze-thaw durability of clogging resistant permeable pavement. 12th International Conference on Concrete Pavements, International Society for Concrete Pavements.

[38] A. Kia, H.S. Wong, C.R. Cheeseman, Freeze-Thaw Durability of Conventional and Novel Permeable Pavement Replacement, Journal of Transportation Engineering, Part B: Pavements 148 (4) (2022) 04022051.

[39] H.K. Kim, J.H. Jeon, H.K. Lee, Workability and mechanical, acoustic and thermal properties of lightweight aggregate concrete with a high volume of entrained air, Construction and Building Materials 29 (2012) 193–200.

[40] Klieger, P. 1956. Effect of Entrained Air on Strength and Durability of Concrete with Various Sizes of Aggregates. Washington, DC: 1-19.

[41] Łaźniewska-Piekarczyk, B., Miera, P. and Szwabowski, J. 2017. "Plasticizer and Superplasticizer Compatibility with Cement with Synthetic and Natural Air-Entraining Admixtures." *Materials Scince and Engineering* 245 (032094).

[42] H. Liu, G. Luo, Y. Gong, H. Wei, Mechanical Properties, Permeability, and Freeze-Thaw Resistance of Pervious Concrete Modified by Waste Crumb Rubbers, Applied Sciences 8 (10) (2018) 1843.

[43] K. Liu, J. Yan, Q. Hu, Y. Sun, C. Zou, Effects of parent concrete and mixing method on the resistance to freezing and thawing of air-entrained recycled aggregate concrete, Construction and Building Materials 106 (2016) 264–273.

[44] L.A. Mata, M.L. Leming, Vertical distribution of sediments in pervious concrete pavement systems, ACI Materials Journal 109 (2) (2012) 149–155.

[45] P.K. Mehta, P.J.M. Monteiro, Concrete: Microstructure, Properties, and Materials, McGraw-Hill Education, New York, 2014.

[46] S. Mondal, K.P. Biligiri, Crumb Rubber and Silica Fume Inclusions in Pervious Concrete Pavement Systems: Evaluation of Hydrological, Functional, and Structural Properties, Journal of Testing and Evaluation 46 (3) (2018) 892–905.

[47] A.M. Neville, J.J. Brooks, Concrete technology, Longman Scientific & Technical England, 1987.

[48] NRMCA 2004. *Freeze Thaw Resistance of Pervious Concrete*. MD20910. National Ready Mixed Concrete Association (NRMCA): 1-16.

[49] Otto, et al., Climate change increases the probability of heavy rains, Environmental Research 13 (2018) 1–12.

[50] F. Özcan, M.E. Koc, Influence of ground pumice on compressive strength and air content of both non-air and air entrained concrete in fresh and hardened state, Construction and Building Materials 187 (2018) 382–393.

[51] C. Ozyildirim, Air-void characteristics of concretes in different applications, Transportation Research Record 1893 (1) (2004) 70–74.

[52] N. Puthipad, M. Ouchi, A. Attachaiyawuth, Effects of fly ash, mixing procedure and type of air-entraining agent on coalescence of entrained air bubbles in mortar of self-compacting concrete at fresh state, Construction and Building Materials 180 (2018) 437–444.

[53] S. Rath, M. Ouchi, N. Puthipad, A. Attachaiyawuth, Improving the stability of entrained air in self-compacting concrete by optimizing the mix viscosity and air entraining agent dosage, Construction and Building Materials 148 (2017) 531–537.

[54] Richardson, M. 2007. *8 - Degradation of concrete in cold weather conditions. Durability of Concrete and Cement Composites*. C. L. Page and M. M. Page, Woodhead Publishing: 282-315.

[55] M.A.A. Salem, R. Pandey, Effect of air entrainment on compressive strength, density, and ingredients of concrete, Int. J. of Advances in Mech. and Civil Eng 4 (6) (2017) 77–81.

[56] Schaefer, V. R., Wang, K., Suleiman, M. T. and Kevern, J. T. 2006. *Mix Design Development for Pervious Concrete In Cold Weather Climates*. Ames, Iowa, USA, Iowa Department of Transportation: 2006-2001.

[57] Y. Sha, R. Li, Experimental effect of air-entraining agent on the bonding performance of concrete under freeze-Thaw cycling, Boletin Tecnico/Technical Bulletin 55 (2017) 179–186.

[58] H.-S. Shang, Triaxial T-C–C behavior of air-entrained concrete after freeze–thaw cycles, Cold Regions Science and Technology 89 (2013) 1–6.

[59] M. Sonebi, M.T. Bassuoni, Investigating the effect of mixture design parameters on pervious concrete by statistical modelling, Construction and Building Materials 38 (2013) 147–154.

[60] M.S. Sumanasooriya, O. Deo, N. Neithalath, Particle packing-based material design methodology for pervious concretes, ACI Materials Journal 109 (2) (2012) 205–213.

[61] J. Szwabowski, B. Lazniewska-Piekarczyk, Air-entrainment problem in self-compacting concrete, Journal of Civil Engineering and Management 15 (2) (2009) 137–147.

[62] N. Tebbal, Z.E.A. Rahmouni, L.R. Chadi, Study of the Influence of an Air-Entraining Agent on the Rheology of Motars, MATEC Web of Conferences, EDP Sciences. 149 (2018) 01054.

[63] M. Toutanji, Technical note The influence of air entrainment on the properties of silica fume concrete, Advances in Cement Research 10 (3) (1998) 135–139.

[64] R. Wang, Z. Hu, Y. Li, K. Wang, H. Zhang, Review on the deterioration and approaches to enhance the durability of concrete in the freeze–thaw environment, Construction and Building Materials 321 (2022), 126371.

[65] H.S. Wong, N.R. Buenfeld, Patch microstructure in cement-based materials: Fact or artefact? Cement and Concrete Research 36 (5) (2006) 990–997.

[66] World Resources Institute 2020. *Trillions in Property at Risk from Flooding*.

[67] Z. Wu, N.A. Libre, K.H. Khayat, Factors affecting air-entrainment and performance of roller compacted concrete, Construction and Building Materials 259 (2020), 120413.

[68] Q. Yang, P. Zhu, X. Wu, S. Huang, Properties of concrete with a new type of saponin air-entraining agent, Cement and Concrete Research 30 (8) (2000) 1313–1317.

[69] Z. Yang, Freezing and thawing durability of pervious concrete under simulated field conditions, ACI Materials Journal 108 (2) (2011) 187–195.

[70] D. Yavuz, The effect of air entraining agents on compressive strength, International Journal of Civil and Environmental Engineering 10 (12) (2017) 1661–1664.

[71] H. Zhang, P. Gao, Z. Zhang, Y. Pan, W. Zhang, Effects of Parameters of Air-Avid structure on the salt-frost durability of hardened concrete, Applied Sciences 10 (2) (2020) 632.

[72] X.H. Zheng, Q.F. Li, J. Yuan, Y. Ge, The Flexural Strength and Frost Resistance of Air Entrained Concrete, Advanced Engineering Forum 5 (2012) 364–369.

[73] A. Ziaei-Nia, G.-R. Tadayonfar, H. Eskandari-Naddaf, Effect of air entraining admixture on concrete under temperature changes in freeze and thaw cycles, Materials Today: Proceedings 5 (2) (2018) 6208–6216.